Geomechanics and Engineering, *Vol. 34, No. 4 (2023) 381-396*
https://doi.org/10.12989/gae.2023.34.4.381

Pseudostatic analysis of bearing capacity of embedded strip footings in rock masses using the upper bound method

Saeed Shamloo[a] and Meysam Imani*

Geotechnical Engineering Group, Amirkabir Univercity of Technology, Garmsar Campus, Iran

(*Received June 1, 2022, Revised May 28, 2023, Accepted June 30, 2023*)

Abstract. The present paper evaluates seismic bearing capacity of rock masses subjected to loads of strip footings using the upper bound method. A general formula was proposed to evaluate the seismic bearing capacity considering both the horizontal and vertical accelerations of the earthquake and the effects of footing embedment depth simultaneously. Modified Hoek-Brown failure criterion was employed for the rock mass. Some comparisons were made with the available solutions and the finite element numerical models to show the accuracy of the developed upper bound formulations. The obtained results show significant improvement compared to the other available solutions. By increasing the horizontal earthquake acceleration from 0.1 to 0.3, the bearing capacity was reduced by up to 39%, while the effect of the vertical earthquake acceleration depends on its direction. An upward acceleration in the range of zero to 0.2 results in an increase in the bearing capacity by up to 24%, while the downward earthquake acceleration has an adverse effect. Also, by increasing the embedment depth of the footing from zero to 5 times the footing width, the value of seismic bearing capacity was raised about 86%. The obtained results were presented as design tables for use in practical applications.

Keywords: Hoek-Brown; rock mass; seismic bearing capacity; strip footings; upper bound

1. Introduction

Determination of the failure mechanism and the static and seismic bearing capacity of rock masses is an essential issue for engineers and is one of the most exciting challenges in geotechnical engineering. Meyerhof (1951) and Shinohara *et al*. (1960) conducted the first attempts on the seismic bearing capacity for soil beddings. After that, different analytical and numerical solutions were presented by various researchers for calculating the seismic bearing capacity of soil beddings, considering the Mohr-Coulomb failure criterion (Soubra 1999, Wang *et al.* 2001, Keshavarz *et al*. 2011, Johari *et al*. 2017, Ghosh and Debnath 2017, Jahani *et al*. 2018, Li *et al*. 2019, Wu *et al*. 2020, Beygi *et al*. 2020, Chen *et al*. 2022). The results obtained by these researchers show that increasing the horizontal and downward vertical earthquake accelerations reduces the seismic bearing capacity.

Commonly, rock masses contain discontinuities. A few methods can take into account the bearing capacity of jointed rock masses with some specific arrangement of the joints (Prakoso and Kulhawy 2004, Imani *et al*. 2012, Bindlish *et al*. 2012). Widely in rock bearing capacity solutions, the researchers considered rock masses as homogeneous media in which the GSI parameter (Geological Strength Index) represents the degree of fracture of the mass (Yang and Yin 2005, Yang 2009, Saada *et al*. 2008, 2011, Keshavarz and Kumar 2017, AlKhafaji *et al*. 2020, Imani and aali 2020. Shamloo and Imani 2020, 2021). Therefore, this simplified hypothesis was considered in the present study. To the authors' knowledge, the number of studies on the seismic bearing capacity of rock masses is minimal compared to soil beddings. Yang (2009) and Saada *et al*. (2011) investigated the seismic bearing capacity of strip footings near rock slopes using the upper bound method. They used the nonlinear Hoek-Brown failure criterion for the rock mass, which was linearized for application in the upper bound method. This linearization was performed by Yang and Yin (2005) and Yang (2009) using a single line instead of the nonlinear Hoek-Brown failure criterion, while Saada *et al*. (2008, 2011) replaced it with several equivalent lines. However, a literature review shows that the linearization method proposed by Mao *et al*. (2012), i.e., the multi-tangential technique, gives the most accurate results than the two mentioned methods. Ausilio and Zimmaro (2015) considered a log-spiral failure mechanism for developing an upper bound formula for the seismic bearing capacity of rock masses. As a simplification, they used the single-line approach for linearization of the Hoek-Brown criterion. They also proposed an approach for the displacement-based dynamic design of shallow strip footings located close to the edge of homogeneous and isotropic rock slopes. They linearized the nonlinear Hoek-Brown criterion with a single straight line, which reduced the accuracy of the obtained bearing capacity magnitude. Keshavarz *et al*. (2016) investigated the seismic bearing capacity of strip footings on rock masses using the slip line method. They showed that the effect of the horizontal earthquake acceleration on the bearing capacity is significant, while the vertical earthquake

*Corresponding author, Assistant Professor
E-mail: Imani@aut.ac.ir
[a]M.Sc. of Geotechnical engineering

ISSN: 2005-307X (Print), 2092-6219 (Online)

acceleration has a minor effect. Li *et al*. (2019) showed that the upward and downward vertical earthquake accelerations increase and decrease the bearing capacity, respectively. Kumar and Rahaman (2020) showed that for the footings adjacent to rock slopes, increasing the inclination of the slopes results in decreasing the bearing capacity.

In a recent study, Alencar *et al*. (2019) studied the influence of footing shape and base roughness on the bearing capacity of rock masses. Also, Alencar *et al*. (2020) investigated the bearing capacity of shallow foundations on bilayer rock masses. They analyzed the influence of different parameters such as the thickness of rock layers, rock type, uniaxial compressive strength of intact rocks, and quality of rock masses on the bearing capacity.

In reality, the footings are constructed in the depth of the ground. Few studies, like Imani and Aali (2020), Shamloo and Imani (2021), were conducted regarding the effect of embedment on the static bearing capacity of rock masses. Reviewing literature shows that in most previous studies for determining the seismic bearing capacity of rock masses, the effect of the embedment depth was considered by an equivalent surcharge. To the authors' knowledge, there exist few solutions like the Roy and Koul (2022) method, which has the capability of considering the extension of the failure lines through the rock mass above the footing base. The shortage of research in this field was considered in the current research by presenting a comprehensive method that can take into account the effect of the horizontal and vertical seismic accelerations and consider the extension of failure lines through the embedment depth. Such a widespread method can be used in most practical engineering applications. The pseudostatic analyses were performed by considering horizontal and vertical earthquake accelerations, i.e., K_h and K_v. These accelerations were multiplied by the rock mass unit weight in order to produce horizontal and vertical forces applied to the failure mechanism. Also, the Hoek-Brown failure criterion was linearized using the multi-tangential technique to obtain the highest accuracy in the results. Therefore, the main contribution of the present method is its capability to consider the simultaneous effects of the vertical and horizontal earthquake accelerations, the embedment depth of the footing, and the most proficient linearization method of the Hoek-Brown criterion. As a particular case, the effect of the proximity of a rock slope to the bearing capacity was investigated by the seismic bearing capacity formula developed in the present study. The effect of superposition in calculating the bearing capacity factors was also investigated.

2. Modified Hoek-Brown failure criterion

The general form of the modified Hoek-Brown failure criterion (Hoek *et al*. 2002), which was implemented in the present study, is as follows

$$\sigma_1 = \sigma_3 + \sigma_{ci}\left(\mathrm{m}_b \frac{\sigma_3}{\sigma_{ci}} + \mathrm{s}\right)^a \tag{1}$$

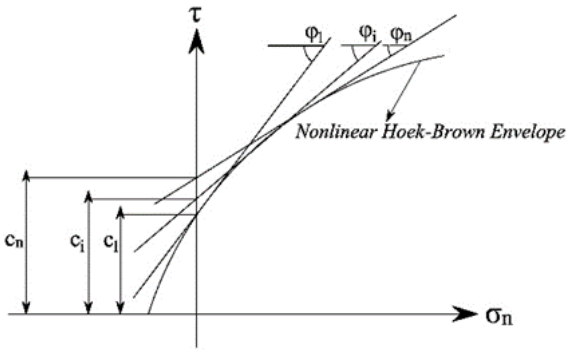

Fig. 1 The multi-tangential technique

Where σ_1 and σ_3 are the major and minor principal stresses at failure, respectively, σ_{ci} is the uniaxial compressive strength of the intact rock. As given in Eqs. (2) to (4), m_b is a reduced value (for the rock mass) of the material constant m_i (for the intact rock), and s and a are the rock mass material constants that depend upon the characteristics of the rock mass

$$m_b = m_i \exp\left(\frac{GSI - 100}{28 - 14D}\right) \tag{2}$$

$$s = \exp\left(\frac{GSI - 100}{9 - 3D}\right) \tag{3}$$

$$a = 1/2 + 1/6\left(\mathrm{e}^{-GSI/15} - \mathrm{e}^{-20/3}\right) \tag{4}$$

Where m_i is a constant parameter for the intact rocks that varies from 4 for weak rocks to 33 for coarse igneous light-colored rocks. D is the disturbance coefficient, which varies from zero for undisturbed in situ rock masses to 1.0 for very disturbed rock masses. GSI is the geological strength index of the rock masses. Researchers proposed various methods to incorporate the nonlinear Hoek-Brown criterion in the bearing capacity problem (Yang and Yin 2005, Saada *et al*. 2008, Mao *et al*. 2012). As stated earlier, Yang and Yin (2005) replaced the nonlinear criterion with a tangential line. Its y-axis intercept is defined as the tangential cohesion, c_t, and its angle with the horizontal direction is defined as the tangential friction angle, φ_t. The φ_t was inserted into the ultimate bearing capacity equation as an unknown parameter, and its value was obtained during an optimization process. Then, the value of the c_t can be obtained as follows

$$c_t = \frac{\sigma_{ci}\cos\varphi_t}{2}\left[\frac{ma(1-\sin\varphi_t)}{2\sin\varphi_t}\right]^{\frac{a}{1-a}} - \frac{\sigma_{ci}\tan\varphi_t}{m}\left(1+\frac{\sin\varphi_t}{a}\right)\left[\frac{ma(1-\sin\varphi_t)}{2\sin\varphi_t}\right]^{\frac{1}{1-a}} + \frac{\sigma_{ci}s}{m}\tan\varphi_t \tag{5}$$

As stated before, the multi-tangential technique proposed by Mao *et al*. (2012) is the best available method for the linearization of the Hoek-Brown criterion in which the nonlinear Hoek-Brown criterion is linearized with several tangential lines, each of them has a unique value of φ_t and c_t. In this method, each velocity vector in the failure mechanism has an exclusive inclination with respect to its corresponding discontinuity line, which means that the φ_t along each of them is unique. Therefore, each discontinuity

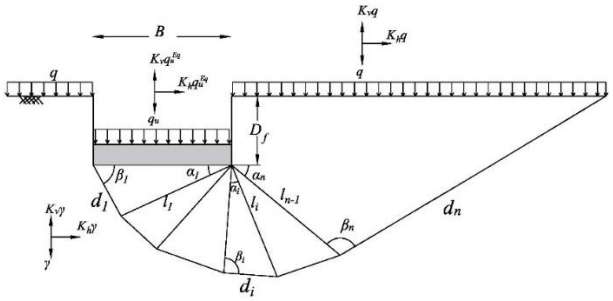

Fig. 2 Nonsymmetrical failure mechanism for determining the seismic bearing capacity of rock masses

line has an individual tangential cohesion. The general configuration of the multi-tangential technique is shown in Fig. 1. Because of its accuracy, this technique was applied in the present study.

3. Calculation of the seismic bearing capacity

3.1 Failure mechanism

Fig. 2 shows the multi-wedge failure mechanism considered in the present paper in which the plastic area under the footing was divided into several wedges, each moving as a rigid block. The mechanism is nonsymmetrical due to the earthquake effect, and it consists of several triangular wedges and a quadrilateral wedge extending up to the ground surface. The total number of wedges, the footing width, and the embedment depth was shown by n, B, and D_f, respectively. Also, the horizontal and vertical accelerations of the earthquake were shown by K_h and K_v, respectively. This mechanism can consider the extension of the failure line through the embedment depth, i.e., the rock mass above the footing base, which was not considered previously in any of the available methods for the seismic bearing capacity of rock masses. Considering the embedment depth, both the weight of the rock mass above the footing base and the mobilized shear strength along the parts of the failure line, which are located above the footing base, were incorporated into the bearing capacity formula.

The shear strength mobilized in the sides of the footing, which are in contact with the surrounding rock mass, was ignored in this research. Also, the effect of surcharge, q was considered in the failure mechanism. Fig. 3 shows the velocity field and the corresponding hodograph of the failure mechanism. According to Fig. 3(a), each wedge has an absolute velocity (V_i) and a relative velocity ($V_{i,\,i+1}$), which inclines with the corresponding failure lines at an angle equal to φ_i and $\varphi_{i,\,i+1}$, respectively. Assuming the associated flow rule for the rock mass, the dilation angle was considered equal to the rock mass friction angle.

3.2 The principle of virtual work

The upper bound method is based on the principle of virtual work in which failure occurs when the work performed by the external forces is greater than or equal to the internal energy dissipated in the failure mechanism. Therefore, to derive the upper bound of the seismic bearing capacity, the external work and the internal energy dissipated in the mechanism should be calculated.

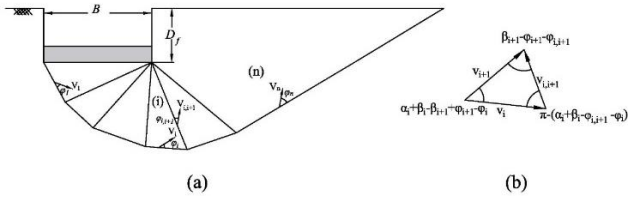

Fig. 3 (a) The Velocity field and (b) The velocity hodograph

3.2.1 Calculation of the external work

The external works are induced by the weight of the rock mass in motion, the surcharge, the footing pressure, and the earthquake horizontal and vertical accelerations. Therefore, the total external work acting on the mechanism was obtained as follows

$$W_{ext} = \sum_{i=1}^{n} W_i + W_q + W_{qu} \tag{6}$$

In which W_i is the work of the weight of the wedge i, W_q is the work performed by the surcharge, and W_{qu} is the work of the footing pressure. It should be emphasized that the effects of both the static and seismic components were considered in determining W_i, W_q, and W_{qu}.

3.2.2 Calculation of the internal energy dissipation

The internal energy dissipates along each velocity discontinuity line, and its magnitude can be calculated by multiplying the length of the discontinuity line by the tangential cohesion and the corresponding velocity magnitude along it. As a result, the amount of internal energy dissipated in the whole mechanism was obtained as follows

$$W_{\text{int}} = \sum_{i=1}^{n} (c_i d_i V_i \cos\varphi_i) + \sum_{i=1}^{n} (c_{i,i+1} l_i V_{i,i+1} \cos\varphi_{i,i+1}) \tag{7}$$

Where V_i is the velocity of the i^{th} wedge, $V_{i,\,i+1}$ is the relative velocity of the wedges i and i+1, c_i, and $c_{i,\,i+1}$ are the tangential cohesions along the lines d_i and l_i, respectively.

3.3 The equation of the ultimate bearing capacity

By equating the total external work and the internal energy dissipated in the whole mechanism, the equation of the seismic bearing capacity of rock masses was obtained as follows

$$q_u^{Eq} = s^{0.5}\sigma_{ci} N_\sigma^{Eq} + qN_q^{Eq} + \frac{1}{2}\gamma B N_\gamma^{Eq} \tag{8}$$

Where N_σ^{Eq} , N_q^{Eq} and N_γ^{Eq} are the seismic bearing capacity factors, which are as follows

$$N_{\sigma}^{Eq}=\frac{(g_1+g_2+g_3)}{(1-K_v)\sin(\beta_1-\varphi_1)+K_h\cos(\beta_1-\varphi_1)} \quad (9)$$

$$N_{q}^{Eq}=\frac{(1-K_v)(g_4+g_5)+K_h(g_6+g_7)}{(1-K_v)\sin(\beta_1-\varphi_1)+K_h\cos(\beta_1-\varphi_1)} \quad (10)$$

$$N_{\gamma}^{Eq}=\frac{(1-K_v)(g_8+g_9+g_{10})+K_h(g_{11}+g_{12}+g_{13})}{(1-K_v)\sin(\beta_1-\varphi_1)+K_h\cos(\beta_1-\varphi_1)} \quad (11)$$

Where g_1 to g_{13} are dimensionless parameters that can be computed from the equations in the appendix.

3.4 Optimization

The developed bearing capacity equation contains some unknown parameters, including the angles α_i, β_i, φ_i and $\varphi_{i,i+1}$. Therefore, considering n wedges for the failure mechanism, the total number of the unknown parameters in the bearing capacity equation equals $4n$. The value of these unknown parameters should be obtained in an optimization process such that the best (lowest) value of the ultimate bearing capacity be achieved. The genetic algorithm tool provided in MATLAB program was used for optimization. Genetic algorithm (GA) is classified as a search heuristic that is used to find approximate solutions to optimization problems. The algorithm creates a population of solutions and applies different operators in order to find the optimized solution to the objective function, which is the bearing capacity formula in the current paper. The procedure to reach the best solution in GA can be summarized as follows:

1. Generating an initial set of solutions, called population.
2. Evaluating the potential solutions to the optimization problem, called chromosomes, in the population.

2.1 Preferentially transferring the fittest chromosomes to the next iteration of the optimization process, called generation.

2.2 Applying GA operators, called cross over and mutation function, for creating new chromosomes.

3. Repeat step 2 until stopping criterion is meet.
4. Return the best chromosome as the solution.

For the final shape of the failure mechanism to be kinematically admissible, the following constraints were taken into account during the optimization:

$\sum_{i=1}^{n}\alpha_i=\pi$, $\alpha_i+\beta_i<\pi$, $\alpha_i+\beta_i>\beta_{i+1}$, $0<\alpha_i+\beta_i-\beta_{i+1}-\phi_i+\phi_{i+1}<\pi$, $\beta_{i+1}-\phi_i-\phi_{i,i+1}>0$, $0<\alpha_i, \phi_i, \phi_{i,i+1}<\pi/2$, $0<\beta_i<\pi$

4. Result and discussions

4.1 Determining the optimal number of wedges in the failure mechanism

Due to the high magnitude of the uniaxial compressive strength of intact rocks, the value of the first part of the bearing capacity formula, i.e., Eq. (8), is considerably higher than the values of the other two parts, which reflects the effect of the surcharge and the weight of the rock mass. Therefore, previous researchers have generally ignored the effects of these two parts in calculating the bearing capacity (Yang and Yin 2005, Saada *et al*. 2011, AlKhafaji *et al*. 2020, Shamloo and Imani 2020, 2021). A calculation example is presented late in this paper in order to verify this assumption. As a result, for a weightless rock mass (γ=0) and in the absence of surcharge load (q=0), the equation of the seismic bearing capacity becomes as follows

$$q_u^{Eq}=s^{0.5}\sigma_{ci}N_{\sigma}^{Eq} \quad (12)$$

Therefore, the seismic bearing capacity factor N_{σ}^{Eq} can be obtained as follows

$$N_{\sigma}^{Eq}=\frac{q_u^{Eq}}{s^{0.5}\sigma_{ci}} \quad (13)$$

The first step in using the upper bound formulation developed in the present paper is to select the optimal number of the wedges, n in the failure mechanism so that the lowest possible value of the seismic bearing capacity be achieved. Assuming σ_{ci} = 10 MPa, GSI = 30, m_i = 10, γ = 0, q = 0, two cases were examined, which include case (I): K_h = K_v = 0 and case (II): K_h = 0.2 and K_v = 0.1. Table 1 presents the variation of N_{σ}^{Eq} in terms of n for these two cases. As can be seen, increasing n results in decreasing N_{σ}^{Eq}. The difference between two successive n values decreases gradually and at n = 9, falls under 1%. Therefore, the optimized value of n = 9 was considered in the following sections of the present paper. It should be mentioned that in previous studies regarding the static bearing capacity of rock masses, the optimal number of wedges was also obtained equal to 9 (AlKhafaji *et al*. 2020, Shamloo and Imani 2020, 2021). Note that this optimal number of n is governed by the linearization technique, not the existence of the earthquake coefficients.

Table 1 Variation of N_{σ}^{Eq} with n

n	Case (I)		Case (II)	
	N_{σ}^{Eq}	Difference (%)	N_{σ}^{Eq}	Difference (%)
2	15.641	-	15.797	-
3	14.216	9.11	13.168	19.96
4	12.939	8.98	11.841	11.2
5	12.423	3.98	10.968	7.97
6	12.116	2.47	10.479	4.66
7	11.934	1.5	10.237	2.36
8	11.778	1.3	10.135	1.01
9	11.746	0.27	10.099	0.36

4.2 Verification

4.2.1 The case of $K_h > 0$

Fig. 4 shows a comparison among the N_{σ}^{Eq} obtained from the present study and that presented by Yang (2009), Saada *et al*. (2011) and Roy and Koul (2022). The trend of variation of N_{σ}^{Eq} in the three mentioned methods is

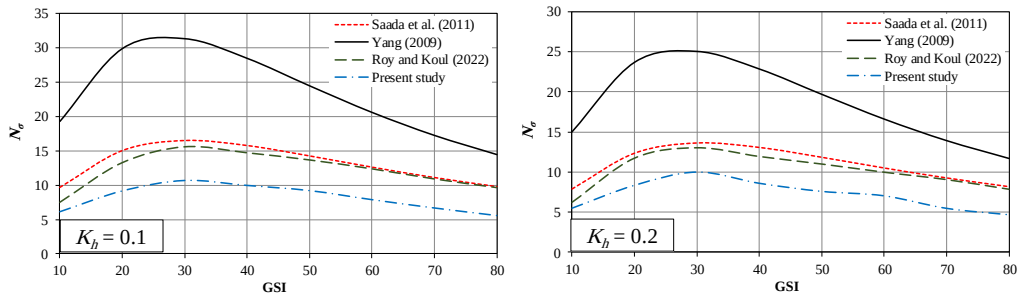

Fig. 4 Comparison of N_σ^{Eq} obtained from the present study and the other methods

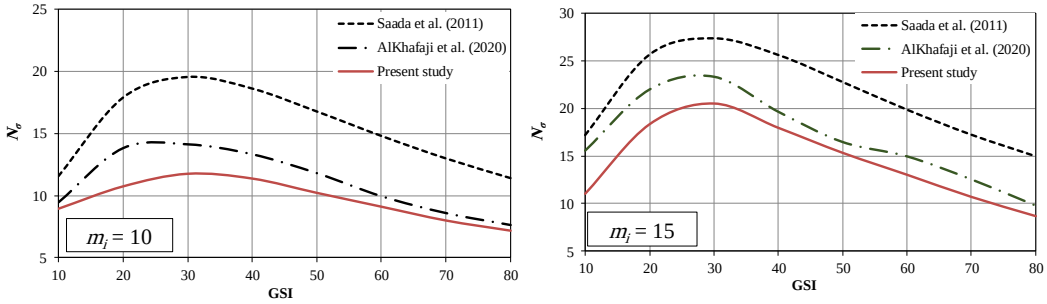

Fig. 5 Comparison of N_σ obtained by different methods assuming K_h = 0

Table 2 Values of N_σ, assuming D=0, σ_{ci}=10MPa, D_f/B=0

	GSI								
m_i	10	20	30	40	50	60	70	80	90
7	6.351	8.389	8.833	8.432	7.526	7.331	6.156	5.963	5.352
10	8.936	10.732	11.746	11.362	10.213	9.236	7.951	7.173	5.969
15	11.032	18.336	20.516	17.819	15.334	13.324	10.703	8.682	8.371
17	13.402	21.503	22.107	21.615	18.972	16.884	12.342	11.638	9.969
25	22.763	30.363	36.862	29.126	21.633	19.162	15.633	13.486	11.021

approximately similar to each other; however, the N_σ^{Eq} values derived from the present study are considerably less than those obtained from the other methods, which shows the efficiency of the presented method in the framework of the upper bound limit analyses. As discussed earlier, the multi-tangential technique used in the present study gives a better approximation of the nonlinear Hoek-Brown criterion, which results in a considerable reduction of the N_σ^{Eq} comparing to the methods of Yang (2009), Saada *et al.* (2011), Roy and Koul (2022).

4.2.2 The case of K_h = 0

As discussed previously, few studies are available for the seismic bearing capacity of rock masses; two of them were used in the previous section for validation of the results of the present study. For further verification, the bearing capacity factor for the case of K_h = 0 was compared to the existing methods proposed for static conditions. In such cases, the failure mechanism should be symmetric, and the nonsymmetrical mechanism used in the present paper (Fig. 2) is inappropriate. However, Saada *et al.* (2011) concluded that relevant results could be obtained using a nonsymmetrical failure mechanism for the static loading condition, i.e., K_h = 0. Therefore, as another verification, assuming $K_h = K_v = 0$ in Eq. (13), the method proposed in the present paper was compared with Saada *et al.* (2011) and AlKhafaji *et al.* (2020) methods, which in the latter, a symmetrical failure mechanism was considered. Since this case corresponds to the static analysis of the bearing capacity, the bearing capacity factor was introduced as N_σ instead of N_σ^{Eq}. It was assumed that σ_{ci} = 10 MPa and D=0.

As shown in Fig. 5, the variation trend of N_σ is almost similar in all methods. However, the present paper results in smaller N_σ than the other methods due to the linearization technique used in the present study, which is more valuable in view of the upper bound method.

For practical applications, Table 2 presents the values of N_σ obtained from the current study, which can be used in practical applications for the case of $K_h = K_v = 0$.

4.2.3 Comparison with the Numerical methods

Using an upper bound solution, the determination of the bearing capacity is much simpler than the finite element method (FEM). In the upper bound method, the bearing capacity can be easily obtained using a formula. In contrast, in a finite element-based program, one should interpret the pressure-settlement curve of a point beneath the footing to estimate the bearing capacity. However, the results of the upper bound method presented in this paper were compared with the finite element method using Phase2 software. For

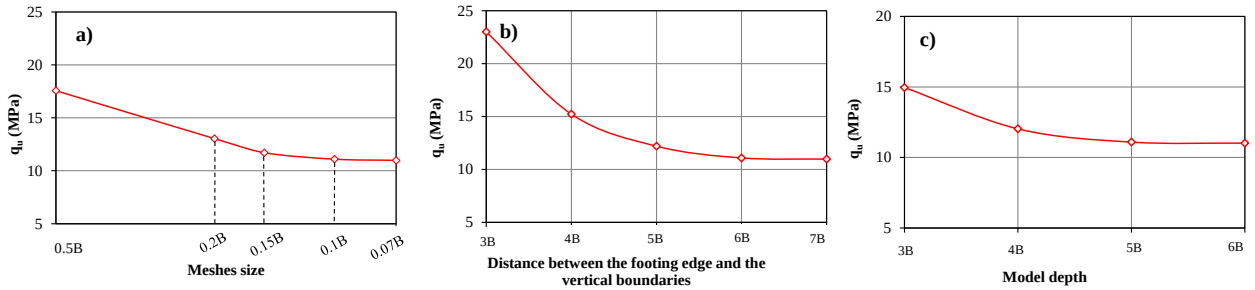

Fig. 6 Variation of q_u versus (a) meshes size, (b) distance between the footing edge and the vertical boundaries of the model, and (c) model depth, considering σ_{ci} = 10 MPa, m_i = 10, GSI = 50, D = 0, B = 1 m, K_h = 0.2, K_v = 0.1 and γ = 21 kN/m^3

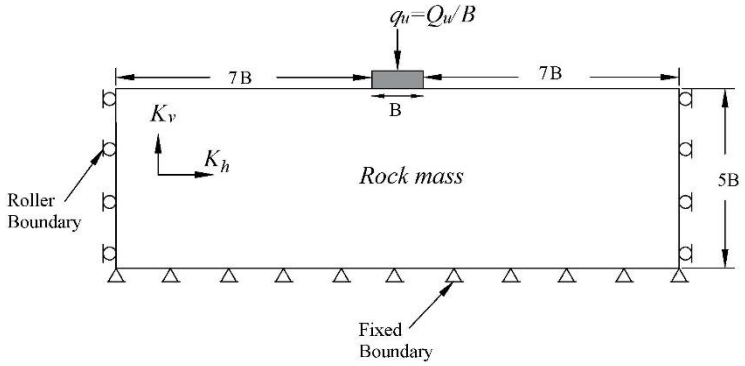

Fig. 7 The geometry and boundary conditions of the finite element models

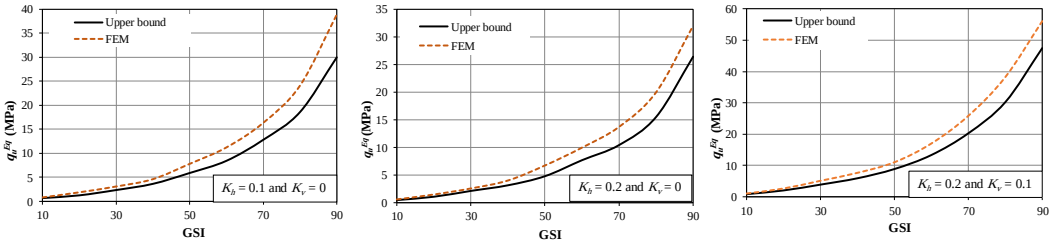

Fig. 8 Comparison of the bearing capacity obtained from the upper bound method and the FEM

determining the bearing capacity from Phase2, an incremental pressure was applied to the ground surface in length equal to the width of the footing (B), and the incremental settlement of a point located below the center of the footing was recorded. Then, the pressure-settlement curve of the point was drawn, and the bearing capacity was calculated using the tangent intersection method (Trautmann and Kulhawy 1998). The meshes' size and the distance of the finite element model boundaries from the footing were determined by trial and error so that the values beyond the determined magnitude do not affect the seismic bearing capacity. As an example, the results of such a trial-and-error procedure were shown in Fig. 6. By decreasing the meshes size (Fig. 6(a)), increasing the distance between the footing edge and the vertical boundaries of the model (Fig. 6(b)), and increasing the model depth (Fig. 6(c)), q_u decreases until reaching an approximately constant magnitude. Therefore, the meshes' size were considered equal to 0.1B, while the distance between the footing edge and the vertical boundaries of the model and the depth of the model were selected equal to 7B and 5B, respectively.

The final geometry and boundary conditions of the FEM models were shown in Fig. 7, in which Q_u is the ultimate failure load (per unit length). The displacement of the vertical boundaries was fixed in the horizontal direction, while the lower boundary was prevented from displacing in both vertical and horizontal directions. Six-noded triangular meshes were used in the models. Assuming σ_{ci} = 10 MPa, m_i = 10, D = 0, B = 1 m, and γ = 21 kN/m^3, Fig. 8 compares the upper bound and the finite element methods for three different combinations of K_h and K_v magnitudes. The results show that the upper bound method provides smaller values of the seismic bearing capacity than the finite element method, which is more appropriate for practical purposes. In the cases of K_h = 0.1 and K_v = 0, K_h = 0.2 and K_v = 0, and K_h = 0.2 and K_v = 0.1, the maximum difference between the q_u^{Eq} of the two methods is 29%, 21%, and 19%, respectively, which was occurred in GSI = 90.

Fig. 9 shows the shear strain contours and the displacement vectors beneath the footing for the ultimate loads. As can be seen, the shear zone was formed nonsymmetrical, which is similar to the configuration of the

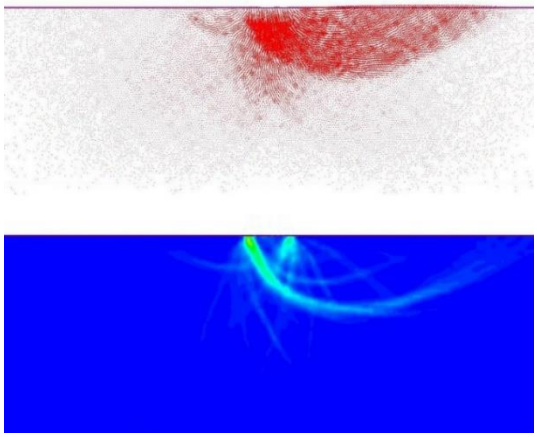

Fig. 9 Shear strain contours and the displacement vectors

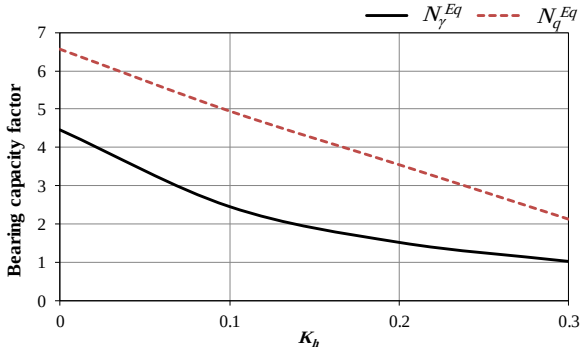

Fig. 10 Effect of K_h on the bearing capacity factors N_q^{Eq} and N_γ^{Eq}, assuming $D_f = 0$ and $B = 1$ m

failure mechanism considered in the upper bound analysis of the present paper.

4.3 Determination of the N_q^{Eq} and N_γ^{Eq} factors

According to Eqs. (10) and (11), and the coefficients g_4 to g_{13} in the appendix, the bearing capacity factors N_q^{Eq} and N_γ^{Eq} are not affected by the Hoek–Brown parameters. Fig. 10 shows the variation of these factors versus K_h. As can be seen, the values of N_q^{Eq} and N_γ^{Eq} decrease with increasing K_h, which results in decreasing the corresponding seismic bearing capacity.

5. Parametric study

Extensive parametric studies were performed to investigate the effects of various factors on the N_σ^{Eq}, and the results were presented in the following sections.

5.1 The effect of earthquake accelerations

5.1.1 The effect of horizontal earthquake coefficient

Fig. 11 shows the effect of horizontal earthquake acceleration on the bearing capacity factor considering different properties for the rock mass. It was assumed that σ_{ci} = 10 MPa, D = 0, and K_v = 0. As can be seen, by increasing K_h, the value of N_σ^{Eq} and the corresponding seismic bearing capacity decrease. The results show that for the assumed properties of the rock mass, by an increase equal to 0.1 in the K_h, the maximum reduction of the N_σ^{Eq} is about 21%. Also, increasing the embedment depth of the footing results in a higher N_σ^{Eq} magnitude.

5.1.2 The effect of vertical earthquake acceleration

Fig. 12 shows the variation of N_σ^{Eq} versus K_v considering different properties for the rock mass. It was assumed that σ_{ci} = 10 MPa, D = 0, and K_h = 0. The positive K_v means an upward earthquake occurrence, while the negative K_v reflects a downward earthquake. As can be seen, for the upward earthquake, increasing K_v results in increasing N_σ^{Eq}, while the downward earthquake acceleration has an adverse effect on N_σ^{Eq}. The downward earthquake acts in the same direction as other external forces result in reducing the bearing capacity. For a 0.1 increase of the upward K_v, the maximum increase of N_σ^{Eq} is about 17%, while for the same increase of the downward K_v, the maximum reduction in N_σ^{Eq} is about 11%.

5.1.3 The effect of simultaneous existence of horizontal and vertical earthquake accelerations

Table 3 presents the values of N_σ^{Eq} for the simultaneous existence of K_h and K_v which can easily be used for practical applications.

5.2 The effect of embedment depth on N_σ^{Eq}

In the existing methods of determining the seismic bearing capacity of rock masses, the effect of embedment depth of footings was considered as a surcharge on both sides of the footing, and the extension of the failure lines through the rock mass above the footing was ignored. This approach results in decreasing the accuracy of the obtained seismic bearing capacity. In this paper, the effect of the footing embedment depth was considered directly without replacing it with an equivalent surcharge. Fig. 13 shows the variation of N_σ^{Eq} versus D_f/B considering different magnitudes of earthquake accelerations and rock mass

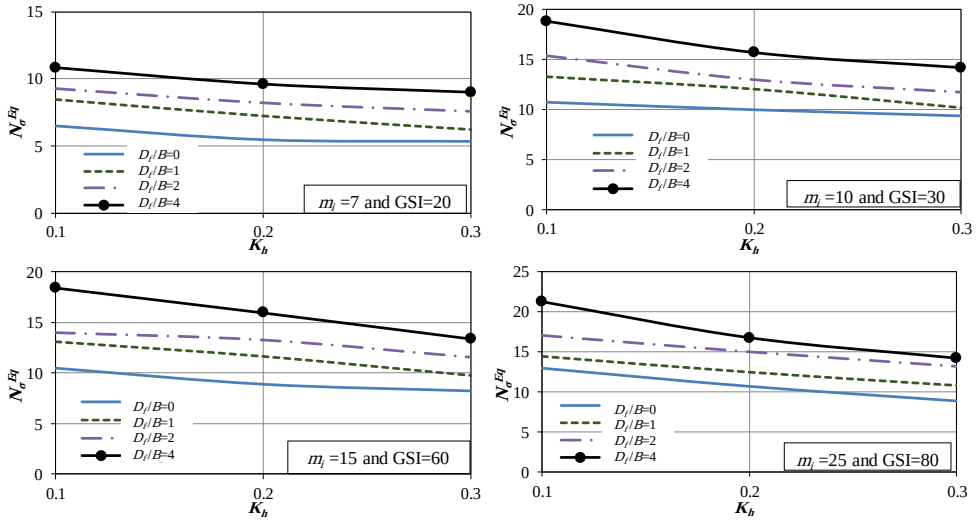

Fig. 11 Variation of N_σ^{Eq} versus K_h

Table 3 Values of N_σ^{Eq} assuming D=0, σ_{ci}=10 MPa, D_f/B=0

m_i	GSI	K_h	K_v	D_f/B				
				0	0.5	1	2	4
7	20	0.1	0.05	7.763	7.862	8.722	9.916	11.726
			0.1	8.716	7.988	8.956	11.186	12.132
		0.2	0.1	6.142	6.699	8.311	8.556	12.963
			0.2	7.855	7.934	8.683	11.075	12.088
		0.3	0.15	6.032	6.466	7.721	8.234	9.826
			0.3	7.303	7.342	7.944	11.012	11.785
10	30	0.1	0.05	10.846	12.763	13.477	15.884	19.116
			0.1	11.554	14.943	15.347	15.963	20.782
		0.2	0.1	10.099	10.703	12.341	14.174	18.226
			0.2	11.056	14.301	15.266	15.563	19.05
		0.3	0.15	8.488	9.452	10.197	12.997	16.132
			0.3	10.614	11.844	12.922	14.851	18.767
15	60	0.1	0.05	11.469	13.642	13.992	16.392	19.968
			0.1	12.711	12.877	15.193	17.203	20.284
		0.2	0.1	11.177	13.363	13.402	15.463	19.177
			0.2	12.015	12.499	13.543	15.833	19.163
		0.3	0.15	10.655	11.077	11.983	13.488	18.526
			0.3	11.554	12.044	13.263	15.091	18.945
25	80	0.1	0.05	12.923	13.321	15.023	17.285	21.287
			0.1	13.332	16.056	16.552	18.991	25.871
		0.2	0.1	12.693	12.942	14.436	17.136	19.693
			0.2	12.966	14.677	15.197	18.812	25.168
		0.3	0.15	11.715	12.833	13.726	15.337	19.212
			0.3	12.745	14.516	15.021	18.463	24.362

properties. The results show that because of the extension of the failure lines through the rock mass above the footing base, increasing D_f/B results in increasing N_σ^{Eq} and the corresponding seismic bearing capacity. For the assumed parameters, by increasing D_f/B from zero to 5, the minimum and maximum increase of the N_σ^{Eq} is equal to 57% and 95%, respectively.

5.3 The effect of σ_{ci} on N_σ^{Eq}

Most of the results of the current paper were presented using the dimensionless factor N_σ^{Eq}, which is influenced by both the σ_{ci} and q_u^{Eq} parameters (see Eq. (13)). Therefore, the magnitude of σ_{ci} does not have a considerable effect on the N_σ^{Eq} since it affects the q_u^{Eq} simultaneously. These two parameters, i.e., σ_{ci} and q_u^{Eq}, neutralize each other's effects according to Eq. (13). Table 4 shows the ignorable influence of σ_{ci} on N_σ^{Eq}. By increasing σ_{ci} from 1 MPa to 100 MPa, the N_σ^{Eq} was reduced by less than 5%.

5.4 Simultaneous optimization of N_σ^{Eq}, N_q^{Eq} and N_γ^{Eq}

The simultaneous optimization of the bearing capacity factors has not been paid enough attention in previous

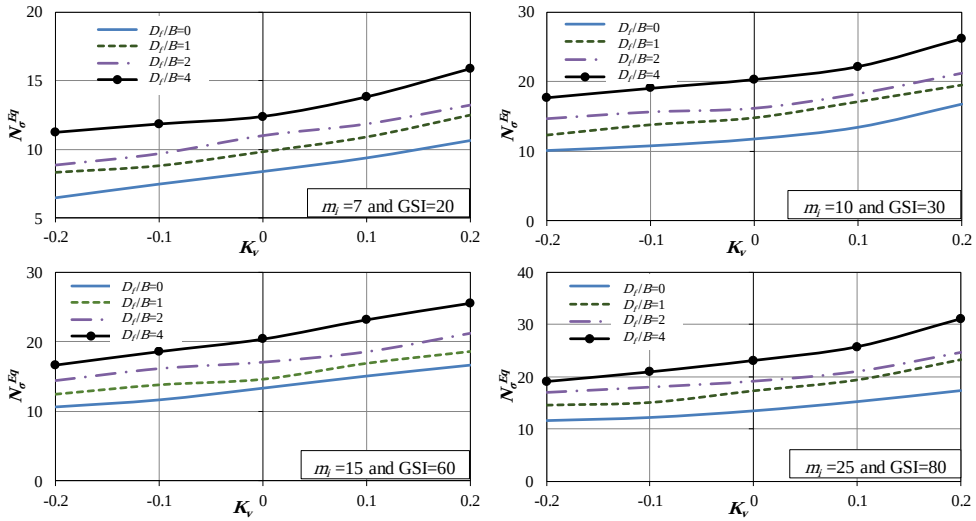

Fig. 12 Variation of N_σ^{Eq} versus K_v assuming B = 1 m

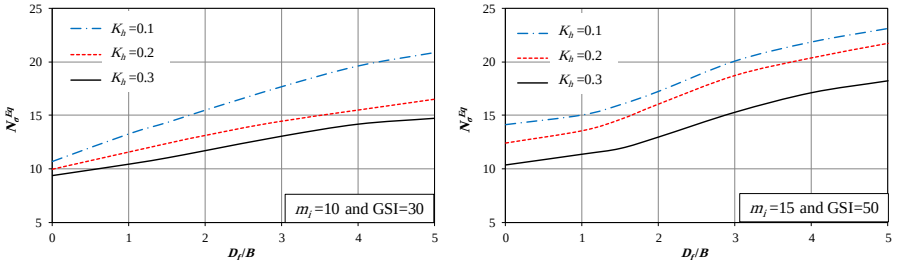

Fig. 13 Variation of N_σ^{Eq} versus D_f/B

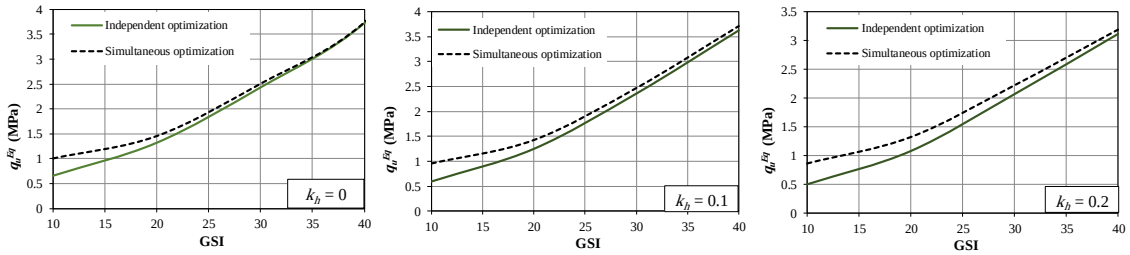

Fig. 14 Comparison of q_u^{Eq} obtained by different optimization methods, assuming m_i = 10, q = 30 kPa, B = 1 m and γ = 21 kN/m^3

Table 4 Variation of N_σ^{Eq} with σ_{ci} assuming m_i = 15, GSI = 30, D = 0, D_f/ B = 2, K_h = 0.1 and K_v = 0.1

σ_{ci} (MPa)	N_σ^{Eq}
1	32.912
2	32.672
5	32.405
10	32.051
25	31.681
50	31.427
100	31.383

studies. In most of the previous researches carried out to calculate the static bearing capacity of rock masses, the principle of superposition was used so that each of the bearing capacity factors in the static condition, i.e., N_σ, N_q, and N_γ, were optimized independently. Then, these factors were replaced in the bearing capacity equation. For example, N_σ was optimized assuming q = 0 and γ = 0, N_q was optimized assuming σ_{ci} = 0 and γ = 0, and N_γ was optimized by assuming σ_{ci} = 0 and q = 0. Due to the simultaneous existence of the parameters σ_{ci} and γ (and sometimes q) in real engineering projects, this optimization method does not match the real conditions of the problems. Therefore, the effect of simultaneous optimization of the seismic bearing capacity factors, i.e., N_σ^{Eq}, N_q^{Eq} and N_γ^{Eq} on the bearing capacity, was investigated in this section. Assuming m_i = 10, q = 30 kPa, B = 1 m, and γ = 21 kN/m^3, Fig. 14 shows the effect of the optimization method of the bearing capacity factors on the q_u^{Eq}. It is clear that the simultaneous optimization results in higher bearing capacity magnitudes, which leads to a smaller size for the footing. With increasing K_h and decreasing GSI, the difference between the two optimization procedures becomes more sensible. For GSI>40, the difference between the q_u^{Eq} obtained from the two optimization methods becomes

Table 5 Values of N_σ^{Eq} assuming $D_f/B = 0$

K_h	m_i	GSI								
		10	20	30	40	50	60	70	80	90
0.1	7	4.213	6.523	7.469	7.381	6.482	5.741	5.202	5.133	4.462
	10	6.152	9.169	10.682	9.963	9.213	7.899	6.694	5.596	5.201
	15	9.214	14.382	16.781	14.732	12.501	10.483	9.772	8.324	6.803
	17	10.971	17.131	20.169	19.013	13.233	11.716	11.352	11.069	9.416
	25	18.326	25.883	30.765	26.336	18.831	16.032	13.529	12.887	10.111
0.2	7	3.112	5.492	7.381	6.124	5.744	5.054	4.336	3.904	3.663
	10	5.512	8.326	9.955	8.573	7.577	7.032	5.49	4.701	4.607
	15	7.882	11.902	12.942	12.074	10.624	8.901	7.855	6.884	5.592
	17	9.861	15.293	18.124	15.561	12.811	10.492	8.816	6.723	5.916
	25	15.982	21.853	25.261	21.362	17.638	16.762	13.041	10.657	8.627
0.3	7	3.024	5.371	6.136	5.662	5.011	4.406	4.272	3.763	3.502
	10	4.646	7.577	9.361	7.923	7.481	6.772	5.082	4.622	4.571
	15	7.513	11.29	11.336	10.795	10.371	8.242	6.851	6.603	5.541
	17	8.941	14.933	15.693	13.113	11.556	10.211	8.401	6.619	5.843
	25	15.12	15.693	24.731	17.443	17.493	14.156	12.796	8.866	8.501

Table 6 Values of N_σ^{Eq} assuming $D_f/B = 0.5$

K_h	m_i	GSI								
		10	20	30	40	50	60	70	80	90
0.1	7	4.482	7.022	8.216	7.851	7.613	6.882	6.108	5.412	5.072
	10	6.941	10.346	12.489	10.841	9.372	8.812	8.144	7.419	5.754
	15	10.453	15.822	16.784	15.883	14.116	12.496	9.825	8.796	7.282
	17	14.071	18.104	21.115	19.236	15.751	13.955	12.154	10.283	9.003
	25	21.223	29.963	35.601	26.332	21.896	18.942	16.997	13.454	11.272
0.2	7	3.86	6.011	7.46	6.784	6.144	5.577	4.933	4.702	4.351
	10	5.566	8.649	12.055	9.742	8.181	7.699	6.228	5.933	4.902
	15	10.202	13.982	16.521	15.614	12.395	9.588	8.07	7.177	6.223
	17	10.203	16.663	18.593	14.056	13.511	11.521	9.574	7.805	6.981
	25	18.617	24.95	25.381	21.523	20.861	18.531	14.821	11.906	9.482
0.3	7	3.403	5.577	6.146	5.673	5.019	4.401	4.331	3.761	3.506
	10	5.233	8.321	9.379	7.949	7.577	7.543	5.082	4.623	4.574
	15	8.432	11.903	11.992	10.823	10.388	8.499	6.869	6.609	5.596
	17	9.997	14.896	17.443	13.655	11.556	10.218	8.407	6.736	5.844
	25	18.241	21.851	24.736	17.482	17.491	16.766	14.366	8.86	8.502

negligible (less than 3%) due to the reduction in the fractures of the rock mass and, consequently, the domination of the strength of the intact rock fragments. Therefore, for using the upper bound-based methods in practical applications, simultaneous optimization of the bearing capacity factors results in economic savings at the expense of footings, especially in the cases of small values of GSI.

5.5 Design tables for practical applications

Tables 5 to 12 provide N_σ^{Eq} factors for use in practical applications. In preparing these tables, the rock mass was considered weightless, and the surcharges on the ground surface beside the footing were ignored. Also, it was assumed that D = 0 and K_v = 0. Based on the findings mentioned in Table 4, N_σ^{Eq} is not highly affected by the magnitude of σ_{ci}. Therefore, to prevent increasing the number of tables, only the case of σ_{ci} = 10 MPa was considered. The seismic bearing capacity can simply be calculated by substituting the relevant N_σ^{Eq} from Tables 5 to 12 into Eq. (12).

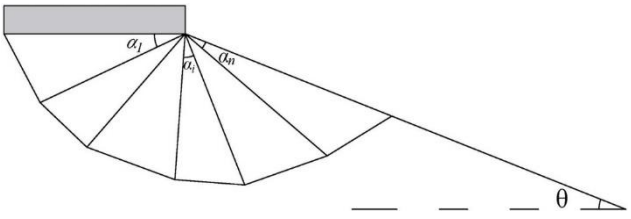

Fig. 15 The case of a footing resting beside a rock slope

5.6 A particular case: the existence of a rock slope

In many mountainous areas, the footings may be adjacent to a rock slope. Therefore, the failure mechanism beneath the footing does not have enough space to be formed, similar to the case of flat ground, which reduces the bearing capacity of rock masses. This particular case can also be solved using the upper bound formulation proposed in the present paper. In this section, the N_σ^{Eq} factor for such a case was investigated. As shown in Fig. 15, it was assumed that the footing is constructed precisely next to a slope, and no gap was considered between the edge of the

Table 7 Values of N_σ^{Eq} assuming $D_f/B = 1$

K_h	m_i	GSI								
		10	20	30	40	50	60	70	80	90
0.1	7	5.196	8.472	9.091	8.594	7.977	7.045	6.607	5.874	5.672
	10	7.574	11.949	13.266	12.437	11.243	9.791	8.597	7.554	6.816
	15	11.981	17.772	18.544	17.536	14.821	13.051	10.155	9.412	8.343
	17	14.216	20.106	21.48	20.016	16.603	14.488	12.297	11.374	9.897
	25	22.856	32.356	35.296	31.144	22.049	21.894	17.896	14.393	11.991
0.2	7	4.352	7.221	7.811	7.466	6.643	6.163	5.844	5.078	4.688
	10	6.363	9.755	12.045	9.861	9.281	7.769	6.736	6.106	5.583
	15	10.341	15.692	17.091	15.709	13.544	11.633	10.109	8.771	7.098
	17	12.711	16.846	21.052	19.793	15.051	14.163	10.202	8.985	7.822
	25	21.277	26.071	26.261	24.923	21.784	19.102	14.956	12.419	10.556
0.3	7	3.791	6.188	7.399	6.533	6.481	5.366	4.921	4.483	4.116
	10	5.156	8.724	10.213	9.163	8.763	7.233	5.994	5.741	4.603
	15	9.126	14.942	15.589	13.452	11.386	9.793	7.693	7.213	5.902
	17	10.066	15.289	17.962	15.266	12.694	10.605	9.574	7.477	6.706
	25	20.322	24.766	25.946	20.933	19.267	17.688	13.713	10.763	9.496

Table 8 Values of N_σ^{Eq} assuming $D_f/B = 1.5$

K_h	m_i	GSI								
		10	20	30	40	50	60	70	80	90
0.1	7	5.633	9.023	10.102	9.844	8.793	7.852	7.133	6.322	6.013
	10	8.194	12.864	14.213	12.956	11.725	9.891	8.882	7.706	7.256
	15	12.882	19.533	20.032	19.193	15.982	13.366	12.072	10.766	9.063
	17	15.011	21.488	22.231	20.094	18.593	15.728	12.496	11.421	10.102
	25	24.763	33.636	36.932	32.722	25.693	22.488	18.462	16.203	12.926
0.2	7	4.455	7.536	8.822	8.544	7.442	6.655	6.225	5.623	5.316
	10	7.054	10.603	12.496	11.202	10.462	9.202	7.416	6.874	6.452
	15	11.231	18.063	18.141	16.952	14.606	12.463	10.339	8.963	7.866
	17	13.501	18.512	21.144	18.271	15.122	14.382	11.317	9.606	8.274
	25	21.402	29.116	30.363	29.082	22.633	20.612	16.868	14.197	11.462
0.3	7	4.321	7.202	7.703	7.102	6.577	5.823	5.188	4.863	4.502
	10	7.386	10.223	11.023	9.482	9.362	8.065	6.682	5.896	5.182
	15	9.725	14.886	17.044	13.992	11.926	11.056	8.684	7.96	6.773
	17	11.872	17.393	19.332	16.523	15.129	11.328	9.493	8.391	8.292
	25	21.102	25.001	26.021	24.233	19.792	18.074	15.102	11.354	10.303

Table 9 Values of N_σ^{Eq} assuming $D_f/B = 2$

K_h	m_i	GSI								
		10	20	30	40	50	60	70	80	90
0.1	7	6.113	9.282	12.244	9.963	9.196	8.726	7.613	7.145	6.356
	10	8.236	12.893	15.366	13.756	12.371	10.719	9.126	8.256	7.341
	15	13.817	21.436	21.977	21.136	17.231	14.002	12.924	10.896	9.716
	17	15.363	23.616	25.416	22.356	19.013	16.873	14.536	11.814	10.49
	25	26.242	38.071	39.156	33.974	27.846	23.377	20.814	17.005	13.437
0.2	7	4.702	8.203	10.099	9.093	8.203	7.366	6.774	5.965	5.574
	10	6.886	12.305	12.966	12.356	11.913	9.439	8.213	7.055	6.716
	15	11.941	16.951	18.741	16.366	14.863	13.282	10.609	8.994	8.566
	17	15.874	20.116	23.106	19.332	16.044	15.374	12.028	10.673	8.703
	25	24.521	31.677	34.79	30.841	27.136	20.832	16.871	14.936	12.094
0.3	7	4.493	7.562	11.593	9.326	6.988	6.442	5.643	5.594	4.772
	10	7.602	11.336	11.702	9.963	9.516	8.674	6.694	6.382	5.916
	15	10.523	15.055	18.956	16.842	12.988	11.596	9.426	8.516	6.932
	17	13.796	17.633	20.263	18.869	14.163	13.471	10.541	10.239	8.116
	25	22.281	28.391	30.301	28.184	20.783	18.983	16.352	13.103	10.437

Table 10 Values of N_σ^{Eq} assuming $D_f/B = 3$

K_h	m_i	GSI								
		10	20	30	40	50	60	70	80	90
0.1	7	6.175	10.002	12.456	11.316	10.303	9.147	8.796	7.881	7.042
	10	8.806	14.951	18.261	15.721	13.308	12.336	9.952	9.116	8.716
	15	15.783	21.466	26.261	22.396	20.226	17.365	13.422	11.513	10.09
	17	19.092	26.447	29.145	23.651	22.051	18.798	14.966	13.243	10.925
	25	30.589	38.975	39.481	34.962	31.284	25.502	23.684	21.063	14.883
0.2	7	5.612	9.163	10.703	10.038	9.788	8.116	7.173	6.714	6.463
	10	7.546	13.895	14.311	14.022	11.714	10.721	10.303	7.993	7.271
	15	13.461	19.226	20.136	19.932	18.719	14.285	12.936	11.874	9.583
	17	16.606	22.446	24.541	23.044	19.826	15.926	14.336	11.945	9.716
	25	25.921	36.032	38.355	32.833	27.522	23.143	19.031	16.041	13.008
0.3	7	4.941	7.916	9.002	9.063	8.362	7.274	7.071	5.992	5.416
	10	7.456	11.383	13.056	12.416	10.816	8.926	7.993	7.291	6.274
	15	12.516	18.764	19.236	18.012	15.293	12.085	11.093	9.206	7.771
	17	15.206	20.063	22.521	18.856	16.326	15.174	12.203	11.725	8.806
	25	23.732	31.994	33.456	29.954	25.806	19.383	17.712	13.674	11.211

Table 11 Values of N_σ^{Eq} assuming $D_f/B = 4$

K_h	m_i	GSI								
		10	20	30	40	50	60	70	80	90
0.1	7	6.532	10.806	13.322	12.305	10.815	10.065	9.045	8.702	8.203
	10	9.521	15.253	18.756	17.346	14.374	12.593	11.306	10.176	9.126
	15	16.191	24.136	26.326	23.942	21.845	18.452	15.574	12.863	11.406
	17	19.342	29.623	29.688	26.573	25.502	20.263	16.203	13.854	12.296
	25	31.596	42.881	43.616	41.605	36.011	27.441	24.129	21.256	16.764
0.2	7	5.689	9.606	11.295	11.115	10.107	9.216	8.177	7.377	6.933
	10	9.326	13.952	15.672	14.124	12.695	11.161	10.987	9.572	7.705
	15	14.674	20.445	24.341	23.914	20.366	15.963	13.272	11.946	10.204
	17	18.672	25.203	28.288	24.556	20.652	18.518	14.763	12.255	10.644
	25	31.203	38.186	41.952	35.762	28.874	25.096	22.743	16.703	14.768
0.3	7	5.174	9.013	9.945	9.541	8.485	7.763	7.012	6.436	6.241
	10	7.974	12.841	14.183	13.903	11.502	10.772	8.674	7.976	7.256
	15	13.882	19.603	20.332	19.405	17.109	13.362	11.196	9.893	9.386
	17	14.546	24.198	23.284	21.956	19.262	15.655	12.682	11.954	9.671
	25	27.242	34.331	36.271	30.542	28.585	22.289	17.893	14.113	13.082

Table 12 Values of N_σ^{Eq} assuming $D_f/B = 5$

K_h	m_i	GSI								
		10	20	30	40	50	60	70	80	90
0.1	7	7.163	12.175	13.592	12.983	12.202	11.742	9.886	9.076	8.296
	10	10.032	17.808	20.884	17.976	15.643	14.965	11.723	11.152	9.752
	15	20.463	26.306	27.103	24.516	22.736	21.415	16.877	13.602	11.852
	17	23.132	30.093	35.352	31.372	25.812	22.293	19.272	15.023	12.785
	25	38.126	46.642	49.632	42.378	36.863	32.318	24.693	23.674	20.926
0.2	7	7.266	10.271	12.077	11.746	10.616	9.751	8.712	8.906	8.136
	10	9.773	14.736	16.362	15.241	14.533	12.223	11.852	9.883	8.546
	15	15.136	23.089	25.936	24.077	21.726	18.125	14.023	12.784	10.352
	17	19.153	26.293	27.623	26.103	24.903	18.714	17.756	15.719	11.373
	25	29.436	39.663	44.416	36.093	31.863	25.746	22.871	19.968	16.519
0.3	7	5.466	10.016	10.863	10.106	9.293	8.126	7.855	7.363	6.626
	10	8.136	13.726	14.732	14.244	11.843	10.925	9.713	8.992	7.372
	15	14.039	22.071	22.413	20.241	18.216	16.056	11.209	12.031	9.621
	17	18.564	25.216	25.169	24.093	19.703	17.163	13.841	12.613	11.277
	25	28.143	36.337	43.751	31.556	29.716	24.371	20.817	18.646	15.954

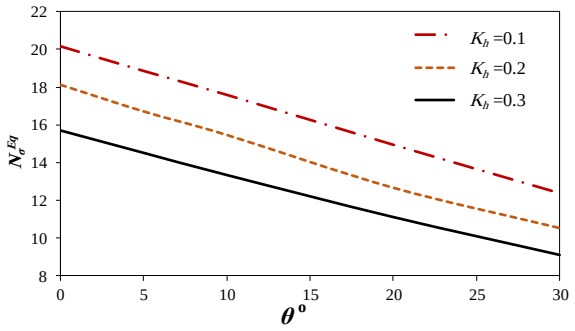

Fig. 16 Variation of N_σ^{Eq} versus θ, assuming m_i = 17, GSI = 30, D_f/B = 0 and K_v = 0

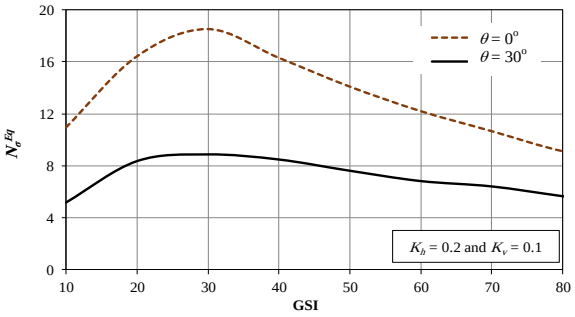

Fig. 17 Variation of N_σ^{Eq}versus GSI, assuming m_i = 10, D_f/B = 0, K_h = 0.2 and K_v = 0.1

footing and the top of the slope. Because of changing the shape of the problem, a new constraint, i.e., $\sum_{i=1}^{n}\alpha_i = \pi - \theta$, was considered instead of the constraint $\sum_{i=1}^{n}\alpha_i = \pi$ previously used for the flat ground condition. Considering K_h = 0.1, 0.2, and 0.3 and assuming K_v = 0, Fig. 16 shows that by increasing the slope of the ground beside the footing, N_σ^{Eq} was reduced due to the reduction of the area of the failure mechanism in the sloping side of the footing. For the three considered values of K_h, by increasing θ from zero to 30°, the maximum reduction of the N_σ^{Eq} is approximately equal to 41%. Fig. 17 shows the influence of θ on the variation of N_σ^{Eq} for the case of $K_h > 0$ and $K_v > 0$. It is clear that increasing θ from zero to 30° results in a considerable reduction of the bearing capacity, which in this particular case, has a maximum value of 52%.

5.7 Solving an example

An example was solved here using the upper bound formula proposed in this paper and other existing solutions. It was assumed that B = 1 m, D_f = 0, σ_{ci} = 20 MPa, m_i = 15, GSI = 50, D = 0, and γ = 26 kN/m^3. The ground slope on one side of the footing was considered equal to 30° concerning the horizontal direction. The seismic bearing capacity was obtained by optimizing Eq. (8) with respect to the unknown parameters. Table 13 compares the seismic bearing capacities obtained from different solutions. Good conformity among the results can be seen. Also, the q_u^{Eq} obtained from the present paper is considerably smaller than the other three methods, which is due to the multi-tangential technique used in the linearization of the Hoek-Brown

Table 13 The q_u^{Eq} for the solved problem

	Yang (2009)	Saada *et al.* (2011)	Ausilio and Zimmaro (2015)	Present study
K_h = 0	25.456	25.430	25.96	21.326
K_h = 0.2	15.438	15.443	15.98	12.537

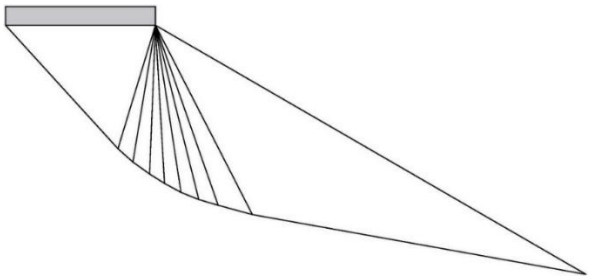

Fig. 18 The final shape of the optimized failure mechanism, assuming K_h = 0.2

criterion. This result is an important advantage of the method proposed in the current paper.

For this example, the unknown parameters of the failure mechanism (i.e., α_i, β_i, φ_i and $\varphi_{i,i+1}$) were obtained from the optimization process, and the corresponding tangential cohesions were derived using Eq. (5). The magnitudes of these parameters were presented in Table 14. Also, the final shape of the failure mechanism is shown in Fig. 18

For the considered case, the bearing capacity factors N_σ^{Eq}, N_q^{Eq} and N_γ^{Eq} became equal to 10.047, 3.456, and 3.302, respectively. Assuming q = 20 kN/m^2, the first, second, and third parts of the bearing capacity equation, i.e., $s^{0.5}\sigma_{ci}N_\sigma^{Eq}$, qN_q^{Eq} and $0.5\gamma BN_\gamma^{Eq}$, becomes equal to 12.494, 0.069, and 0.043, respectively. As stated earlier, this example shows that the first part of the bearing capacity equation plays the most important role in calculating the bearing capacity of rock masses, and the other two parts can be ignored.

6. Conclusions

This paper proposed an analytical solution for determining the seismic bearing capacity of rock masses subjected to the horizontal and vertical earthquake coefficients. The effects of the foundation embedment depth were also investigated. As a particular case, the effect of the proximity of a rock slope on the bearing capacity was studied. The results of this study are as follows:

- Increasing the horizontal coefficient of the earthquake reduces the bearing capacity of rock masses by up to 39%. But the effect of the vertical coefficient depends on its direction. For the upward earthquake, increasing the earthquake coefficient results in increasing the bearing capacity, while the downward earthquake has an adverse effect. A change equal to 0.1 in the upward earthquake coefficient results in 9% to 12% variation of the bearing capacity.
- The horizontal coefficient of the earthquake has a

Table 14 The optimized values of the unknown parameters and the corresponding tangential cohesion, assuming $K_h = 0.2$

n	1	2	3	4	5	6	7	8	9
α_i (°)	73.046	7.566	7.139	5.539	5.441	5.288	5.260	7.933	32.832
β_i (°)	47.561	114.672	116.252	119.841	121.778	120.564	120.354	124.473	127.333
φ_i (°)	33.120	33.730	29.935	32.831	33.480	30.695	36.459	38.230	49.351
$\varphi_{i+1,i}$ (°)	31.770	38.010	36.920	34.113	38.462	41.161	42.215	49.585	45.620

more significant effect on reducing the bearing capacity than the vertical coefficient.

- The seismic bearing capacity of rock masses increases with increasing the embedment of the footings, which is due to the extension of the failure lines through the rock mass above the footing base. For a footing embedded in a depth equal to 5 times its width, the bearing capacity will increase by about 86% compared to the case of the footing resting on the surface of the rock mass.
- Optimizing the whole bearing capacity equation with simultaneous consideration of its three factors results in more economic dimensions of the footings. This type of optimization is not of paramount importance for strong rock masses since in such rocks, the effect of the second and third parts of the bearing capacity equation is negligible compared to the effect of the first part, i.e., N_σ^{Eq}. In contrast, independent optimization of each bearing capacity factor results in bigger footings, which is on the safe side.
- The proximity of a sloping ground to a footing reduces the seismic bearing capacity, which is due to reducing the length of the failure lines and therefore, decreasing the area of the failure wedges in one side of the footing. For every 10° increase in the slope of the ground, approximately 18% reduction of the bearing capacity was observed.

References

Alencar, A.S., Galindo, R.A. and Svetlana, M. (2019), "Bearing capacity of foundation on rock mass depending on footing shape and interface roughness", *Geomech. Eng*., **18**(4), 391-406. https://doi.org/10.12989/gae.2019.18.4.0391.

Alencar, A.S., Galindo, R.A. and Svetlana, M. (2020), "Bearing capacity of shallow foundations on the bilayer rock", *Geomech. Eng*., **21**(1), 11-21. https://doi.org/10.12989/gae.2020.21.1.011.

AlKhafaji, H., Imani, M. and Fahimifar, A. (2020), "Ultimate bearing capacity of rock mass foundations subjected to seepage forces using modified Hoek-Brown criterion", *Rock Mech. Rock Eng.*, **53**, 251-268. http://doi.org/10.1007/s00603-019-01905-6.

Ausilio, E. and Zimmaro, P. (2015), "Displacement-based seismic design of a shallow strip footing positioned near the edge of a rock slope", *Int. J. Rock Mech. Min. Sci.*, **76**, 68-77. https://doi.org/10.1016/j.ijrmms.2015.02.010.

Beygi, M., Keshavarz, A., Abbaspour, M., Vali, R., Saberian, M. and Li, J. (2020), "Finite element limit analysis of the seismic bearing capacity of strip footing adjacent to excavation in c-φ soil", *Geomech. Geoeng*., https://doi.org/10.1080/17486025.2020.1728396.

Bindlish, A., Singh, M. and Samadhiya, N.K. (2012), "Ultimate bearing capacity of shallow foundations on jointed rock mass", *Indian Geotech. J.*, **42**(3), 169-178. https://doi.org/10.1007/s40098-012-0011-9.

Chen, B.H., Lou, W.J., Xu, X.Y. and Hu, R.Q. (2022), "Seismic bearing capacity of strip footing with nonlinear Mohr–Coulomb failure criterion", *Int. J. Geomech.*, **22**(10). https://doi.org/10.1061/(ASCE)GM.1943-5622.0002521.

Ghosh, S. and Debnath, L. (2017), "Seismic bearing capacity of shallow strip footing with coulomb failure mechanism using limit equilibrium method", *Geotech. Geol. Eng.*, https://doi.org/10.1007/s10706-017-0268-y.

Hoek, E., Carranza, C. and Corkum, B. (2002), "Hoek–Brown failure criterion, 2002 edition", *Proceedings of the NARMS-Tac*, 267-273. https://doi.org/10.1016/0148-9062(74)91782 -3.

Imani, M. and Aali, R. (2020), "Effects of embedment depth of foundations on ultimate bearing capacity of rock masses", *Geotech. Geol. Eng*., https://doi.org/10.1007/s10706-020-01452-w.

Imani, M., Fahimifar, A. and Sharifzadeh, M. (2012), "Upper bound solution for the bearing capacity of submerged jointed rock foundations", *Rock Mech. Rock Eng.*, **45**, 639-646. https://doi.org/10.1007/s00603-011-0215-9.

Johari, A., Hosseini, S.M. and Keshavarz, A. (2017), "Reliability analysis of seismic bearing capacity of strip footing by stochastic slip lines method", *Comput. Geotech.*, **91**, 203-217. https://doi.org/10.1016/j.compgeo.2017.07.019.

Jahani, M., Oulapour, M., Haghighi, A. (2018), "Evaluation of the Seismic Bearing Capacity of Shallow Foundations Located on the Two-Layered Clayey Soils", *Iran J Sci Technol Trans Civ Eng*. https://doi.org/10.1007/s40996-018-0122-3.

Keshavarz, A., Jahanandish, M. and Ghahramani, A. (2011), "Seismic bearing capacity analysis of reinforced soils by the method of stress characteristics", *Iran J. Sci. Technol. Trans. Civ. Eng.*, **35**(2), 185-197. https://doi.org/10.22099/IJSTC.2012.666.

Keshavarz, A., Fazeli, A. and Sadeghi, S. (2016), "Seismic bearing capacity of strip footings on rock masses using the HoekeBrown failure criterion", *J. Rock Mech. Geotech. En.g*, **8**, 170-177. https://doi.org/10.1016/j.jrmge.2015.10.003.

Keshavarz, A. and Kumar, J. (2017), "Bearing capacity of foundations on rock mass using the method of characteristics", *Int. J. Numer. Anal. Method. Geomech.*, 1-16. https://doi.org/10.1002/nag.2754.

Kumar, J. and Rahaman, O. (2020), "Lower bound limit analysis using power cone programming for solving stability problems in rock mechanics for generalized Hoek–Brown criterion", *Rock Mech. Rock Eng*., https://doi.org/10.1007/s00603-020-02099-y.

Li, C., Jiang, P. and Zhou, A. (2019), "Rigorous solution of slope stability under seismic action", *Comput. Geotech.*, **109**, 99-107. https://doi.org/10.1016/j.compgeo.2019.01.018.

MATLAB. (R2016a), https://www.mathworks.com.

Mao, N., Al-Bittar, T. and Soubra, A.H. (2012), "Probabilistic analysis and design of strip foundations resting on rocks obeying Hoek–Brown failure criterion", *Int. J. Rock Mech. Min. Sci.*, **49**, 45-58. https://doi.org/10.1016/j.ijrmm s.2011.11.005.

Meyerhof, G.G. (1951), "The ultimate bearing capacity of foundations", *Geotechnique*, **2**(4), 301-332.

https://doi.org/10.1680/geot.1951.2.4.301.
Phase2. Ver.8. (2011), www.rocscience.com.
Prakoso, W.A. and Kulhawy, F.H. (2004), "Bearing capacity of strip footings on jointed rock masses", *J. Geotech. Geoenviron. Eng.*, **130**(12). https://doi.org/10.1061/(ASCE)1090-0241(2004)130:12(1347).
Roy, N. and Koul, S. (2022) "Effect of embedment depth on the seismic bearing capacity of strip footing in rock mass", *Int. J. Geomech.*, **22**(7), 06022010. https://doi.org/10.1061/(ASCE)GM.1943-5622.0002463.
Saada, Z., Maghous, S. and Garnier, D. (2008), "Bearing capacity of shallow foundations on rocks obeying a modified Hoek–Brown failure criterion", *Comput. Geotech.*, **35**, 144-154. https://doi.org/10.1016/j.compg eo.2007.06.003.
Saada, Z., Maghous, S. and Garnier, D. (2011), "Seismic bearing capacity of shallow foundations near rock slopes using the generalized Hoek–Brown criterion", *Int. J. Numer. Anal. Meth. Geomech*., **35**, 724-748. https://doi.org/10.1002/nag.
Shamloo, S., Imani, M. (2020), "Upper bound solution for the bearing capacity of rock masses considering the embedment depth", *Ocean Eng.*, 218(108169). https://doi.org/10.1016/j.oceaneng.2020.108169.
Shamloo, S. and Imani, M. (2021), "Upper bound solution for the bearing capacity of two adjacent footings on rock masses", *Comput. Geotech.*, 129(103855). https://doi.org/10.1016/j.compgeo.2020.103855.
Shinohara, T., Tateishi, T. and Kubo, K. (1960) "Bearing capacity of sandy soil for eccentric and inclined load and lateral resistance of single piles embedded in sandy soil", *Proceedings of the 2nd World Conference on Earthquake Engineering*. Tokyo.
Soubra, A.H. (1999), "Upper-bound solutions for bearing capacity of foundations", *J. Geotech. Geoenviron. Eng.*, **125**(1), 59-68. https://doi.org/10.1061/(ASCE)1090-0241(1999)125:1(59).
Trautmann, C.H. and kulhawy, F.H. (1998), "Uplift Load-Displacement Behavior of Spread Foundations", *J. Geotech. Eng. - ASCE*, **114**(2), 168-183. https://doi.org/10.1061/(ASCE)0733-9410 (1988) 114:2(168).
Wang, Y.J., Yin, J.H. and Chen, Z.Y. (2001), "Calculation of bearing capacity of a strip footing using an upper bound method", *Int. J. Numer. Anal. Meth. Geomech.*, **25**, 841-851. https://doi.org/10.1002/nag.151.
Wu, G., Zhao, H., Zhao, M. and Xiao, Y. (2020), "Undrained seismic bearing capacity of strip footings lying on two-layered slopes", *Comput. Geotech.*, **122**(103539). https://doi.org/10.1016/j.compgeo.2020.103539.
Yang, X.L. and Yin, J.H. (2005), "Upper bound solution for ultimate bearing capacity with a modified Hoek-Brown failure criterion", *Int. J. Rock Mech. Min. Sci.*, **42**, 550-560. https://doi.org/10.1016/j.ijrmms.2005.03.002.
Yang, X.L. (2009), "Seismic bearing capacity of a strip footing on rock slopes", *Can Geotech. J.*, **46**, 943-954. https://doi.org/10.1139/T09-038.

CC

Appendix

a) The length of discontinuity lines and the area of wedges

$$l_i = B\,\frac{\sin\beta_1}{\sin(\alpha_1+\beta_1)}\prod_{j=2}^{i}\frac{\sin(\beta_j)}{\sin(\alpha_j+\beta_j)} \qquad i=1 \text{ to } n\text{-}1$$

$$l_n = D_f\,\frac{\sin(\alpha_n+\beta_n-\frac{\pi}{2})}{\sin(\alpha_n+\beta_n)} + B\,\frac{\sin\beta_1}{\sin(\alpha_1+\beta_1)}\prod_{j=2}^{n}\frac{\sin(\beta_j)}{\sin(\alpha_j+\beta_j)}$$

$$d_i = B\,\frac{\sin\beta_1}{\sin(\alpha_1+\beta_1)}\frac{\sin\alpha_i}{\sin\beta_i}\prod_{j=2}^{i}\frac{\sin(\beta_j)}{\sin(\alpha_j+\beta_j)} \qquad i=1 \text{ to } n\text{-}1$$

$$d_n = \frac{D_f}{\sin(\alpha_n+\beta_n)} + B\,\frac{\sin\beta_1}{\sin(\alpha_1+\beta_1)}\frac{\sin\alpha_n}{\sin\beta_n}\prod_{j=2}^{n}\frac{\sin(\beta_j)}{\sin(\alpha_j+\beta_j)}$$

$$S_i = \frac{B^2}{2}\,\frac{\sin^2\beta_1}{\sin^2(\alpha_1+\beta_1)}\,\frac{\sin\alpha_i\,\sin(\alpha_i+\beta_i)}{\sin\beta_i}\prod_{j=2}^{i}\frac{\sin^2(\beta_j)}{\sin^2(\alpha_j+\beta_j)}$$

i=1 to n-1

$$S_n = \left[\frac{B^2}{2}\,\frac{\sin^2\beta_1}{\sin^2(\alpha_1+\beta_1)}\,\frac{\sin\alpha_n\,\sin(\alpha_n+\beta_n)}{\sin\beta_n}\prod_{j=2}^{n}\frac{\sin^2(\beta_j)}{\sin^2(\alpha_j+\beta_j)}\right] + \left[D_f.B\,\frac{\sin\beta_1}{\sin(\alpha_1+\beta_1)}\prod_{j=2}^{n}\frac{\sin(\beta_j)}{\sin(\alpha_j+\beta_j)}\right] + \left[\frac{D_f{}^2}{2}.\frac{\sin(\alpha_n+\beta_n-\frac{\pi}{2})}{\sin(\alpha_n+\beta_n)}\right]$$

b) The non-Dimensional coefficients g_1 to g_{13}

$$g_1 = \frac{\sin\beta_1}{\sin(\alpha_1+\beta_1)}\times \sum_{i=1}^{n}\left[c_i.\cos\varphi_i.\frac{\sin\alpha_i}{\sin\beta_i}\prod_{j=2}^{i}\frac{\sin\beta_j}{\sin(\alpha_j+\beta_j)}\prod_{j=1}^{i-1}\frac{\sin(\alpha_j+\beta_j-\varphi_j-\varphi_{j,j+1})}{\sin(\beta_{j+1}-\varphi_{j+1}-\varphi_{j,j+1})}\right]$$

$$g_2 = \frac{\sin\beta_1}{\sin(\alpha_1+\beta_1)}\times \sum_{i=1}^{n-1}\left[c_{i,i+1}.\cos\varphi_{i,i+1}.\frac{\sin(\alpha_i+\beta_i-\beta_{i+1}+\varphi_{i+1}-\varphi_i)}{\sin(\beta_{i+1}-\varphi_{i+1}-\varphi_{i,i+1})}\prod_{j=2}^{i}\frac{\sin\beta_j}{\sin(\alpha_j+\beta_j)}.\prod_{j=1}^{i-1}\frac{\sin(\alpha_j+\beta_j-\varphi_j-\varphi_{j,j+1})}{\sin(\beta_{j+1}-\varphi_{j+1}-\varphi_{j,j+1})}\right]$$

$$g_3 = \left(\frac{D_f}{B}\right)\frac{\cos\varphi_n}{\sin(\alpha_n+\beta_n)}c_n\prod_{j=1}^{n-1}\frac{\sin(\alpha_j+\beta_j-\varphi_j-\varphi_{j,j+1})}{\sin(\beta_{j+1}-\varphi_{j+1}-\varphi_{j,j+1})}$$

$$g_4 = \frac{\sin^2\beta_1}{\sin^2(\alpha_1+\beta_1)}\times \sum_{i=1}^{n}\left[\frac{\sin\alpha_i.\sin(\alpha_i+\beta_i)}{\sin\beta_i}\sin(\beta_i-\sum_{j=1}^{i-1}\alpha_j-\varphi_i)\times\prod_{j=2}^{i}\frac{\sin^2\beta_j}{\sin^2(\alpha_j+\beta_j)}.\prod_{j=1}^{i-1}\frac{\sin(\alpha_j+\beta_j-\varphi_j-\varphi_{j,j+1})}{\sin(\beta_{j+1}-\varphi_{j+1}-\varphi_{j,j+1})}\right]$$

$$g_5 = \left(\frac{D_f}{B}\right)\frac{\sin(\alpha_n+\beta_n-\frac{\pi}{2})}{\sin(\alpha_n+\beta_n)}\times \sin(\beta_n-\sum_{j=1}^{n-1}\alpha_j-\varphi_n)\times\prod_{j=1}^{n-1}\frac{\sin(\alpha_j+\beta_j-\varphi_j-\varphi_{j,j+1})}{\sin(\beta_{j+1}-\varphi_{j+1}-\varphi_{j,j+1})}$$

$$g_6 = \frac{\sin^2\beta_1}{\sin^2(\alpha_1+\beta_1)}\times \sum_{i=1}^{n}\left[\frac{\sin\alpha_i.\sin(\alpha_i+\beta_i)}{\sin\beta_i}\cos(\beta_i-\sum_{j=1}^{i-1}\alpha_j-\varphi_i)\times\prod_{j=2}^{i}\frac{\sin^2\beta_j}{\sin^2(\alpha_j+\beta_j)}.\prod_{j=1}^{i-1}\frac{\sin(\alpha_j+\beta_j-\varphi_j-\varphi_{j,j+1})}{\sin(\beta_{j+1}-\varphi_{j+1}-\varphi_{j,j+1})}\right]$$

$$g_7 = \left(\frac{D_f}{B}\right)\frac{\sin(\alpha_n+\beta_n-\frac{\pi}{2})}{\sin(\alpha_n+\beta_n)}\times \cos(\beta_n-\sum_{j=1}^{n-1}\alpha_j-\varphi_n)\times\prod_{j=1}^{n-1}\frac{\sin(\alpha_j+\beta_j-\varphi_j-\varphi_{j,j+1})}{\sin(\beta_{j+1}-\varphi_{j+1}-\varphi_{j,j+1})}$$

$$g_8 = \frac{\sin(\beta_1)}{\sin(\alpha_1+\beta_1)}\times \sin(\beta_n-\varphi_n-\sum_{j=1}^{n-1}\alpha_j)\times\prod_{j=2}^{n}\frac{\sin\beta_j}{\sin(\alpha_j+\beta_j)}\prod_{j=1}^{n-1}\frac{\sin(\alpha_j+\beta_j-\varphi_j-\varphi_{j,j+1})}{\sin(\beta_{j+1}-\varphi_{j+1}-\varphi_{j,j+1})}$$

$$g_9 = \left(\frac{D_f}{B}\right)^2\frac{\sin(\alpha_n+\beta_n-\frac{\pi}{2})}{\sin(\alpha_n+\beta_n)}\times \sin(\beta_n-\sum_{j=1}^{n-1}\alpha_j-\varphi_n).\prod_{j=1}^{n-1}\frac{\sin(\alpha_j+\beta_j-\varphi_j-\varphi_{j,j+1})}{\sin(\beta_{j+1}-\varphi_{j+1}-\varphi_{j,j+1})}$$

$$g_{10} = \frac{D_f}{B}\frac{2\sin\beta_1}{\sin(\alpha_1+\beta_1)}\times \sin(\beta_n-\sum_{j=1}^{n-1}\alpha_j-\varphi_n).\prod_{j=2}^{n}\frac{\sin\beta_j}{\sin(\alpha_j+\beta_j)}.\prod_{j=1}^{n-1}\frac{\sin(\alpha_j+\beta_j-\varphi_j-\varphi_{j,j+1})}{\sin(\beta_{j+1}-\varphi_{j+1}-\varphi_{j,j+1})}$$

$$g_{11} = \frac{\sin(\beta_1)}{\sin(\alpha_1+\beta_1)}\times \cos(\beta_n-\varphi_n-\sum_{j=1}^{n-1}\alpha_j)\times\prod_{j=2}^{n}\frac{\sin\beta_j}{\sin(\alpha_j+\beta_j)}\prod_{j=1}^{n-1}\frac{\sin(\alpha_j+\beta_j-\varphi_j-\varphi_{j,j+1})}{\sin(\beta_{j+1}-\varphi_{j+1}-\varphi_{j,j+1})}$$

$$g_{12} = \left(\frac{D_f}{B}\right)^2\frac{\sin(\alpha_n+\beta_n-\frac{\pi}{2})}{\sin(\alpha_n+\beta_n)}\times \cos(\beta_n-\sum_{j=1}^{n-1}\alpha_j-\varphi_n).\prod_{j=1}^{n-1}\frac{\sin(\alpha_j+\beta_j-\varphi_j-\varphi_{j,j+1})}{\sin(\beta_{j+1}-\varphi_{j+1}-\varphi_{j,j+1})}$$

$$g_{13} = \frac{D_f}{B}\frac{2\sin\beta_1}{\sin(\alpha_1+\beta_1)}\times \cos(\beta_n-\sum_{j=1}^{n-1}\alpha_j-\varphi_n).\prod_{j=2}^{n}\frac{\sin\beta_j}{\sin(\alpha_j+\beta_j)}.\prod_{j=1}^{n-1}\frac{\sin(\alpha_j+\beta_j-\varphi_j-\varphi_{j,j+1})}{\sin(\beta_{j+1}-\varphi_{j+1}-\varphi_{j,j+1})}$$